ISSN 1392-1207. MECHANIKA. Vol. 29, No. 6, 2023: 511–517

Optimization of Motion Parameters and Structural Stiffness of Spatial Four-Bar Weft Insertion Mechanism of Rapier Loom

Menglu XI*, Kaihong ZHOU, Xueqian ZHANG***, Xin LU******

**College of Mechanical and Control Engineering, Guilin University of Technology, Guilin 541006, China, E-mail: xmlachieve@163.com*

***College of Mechanical and Control Engineering, Guilin University of Technology, Guilin 541006, China, E-mail: 510429271@qq.com (Corresponding author)*

****College of Mechanical and Control Engineering, Guilin University of Technology, Guilin 541006, China, E-mail: 992770396@qq.com*

*****College of Mechanical and Control Engineering, Guilin University of Technology, Guilin 541006, China, E-mail: 289661703@qq.com*

https://doi.org/10.5755/j02.mech.33658

1. Introduction

Rapier loom, as a commonly used textile machine, is widely used in the textile industry because of its good reliability, fast rotation speed, high efficiency and strong adaptability [1]. Weft insertion mechanism is one of the important components of rapier loom, its motion stability and precision directly determine the reliability of loom performance and fabric quality, so many scholars have studied the optimization design of weft insertion mechanism.

Zhu Zhichao proposed for the first time the optimization design of the spatial six bar combination weft insertion mechanism by using genetic algorithm, and finally proved that it is feasible to optimize the weft insertion mechanism by using this algorithm. Chen Jianneng proposed an improved genetic algorithm for multiobjective optimization of a novel weft insertion mechanism under complex constraints, and the optimization results met the requirements. Tang Chaofei established a virtual prototype model for the spatial linkage weft insertion mechanism, optimized the structure according to the quality and stiffness, and improved the quality of carbon fiber weft insertion. Zhou Xiangqin proposed to reduce the mass and moment of inertia of the component which accounted for a large part by considering the variation law of the equivalent moment of inertia of the spindle of each component, and adopted the loom prototype for testing and verification. The final results showed that the optimization scheme had a significant effect on reducing loom vibration and improving loom speed.

The GTX plus 4-R190 rapier loom is invented by Picanol in Belgium. The model is equipped with two rear beams. It includes a fixed rear beam for loading and unloading easily. When processing heavy products such as large blankets, fixed back beams are installed to withstand greater pressure. When processing towels, thin denim fabrics and other products, you can remove the fixed rear beams to reduce the weight of the machine. The machine adopts GTM series rapier heads. They can be used for a variety of yarns. SMIT has developed the new ONE rapier loom in Italy. It mainly uses the weft joint rapier with a small cross sectional area to complete weft insertion. The weft joint can be completed at the shed, so there is no need for too large shed. As a result, the selection of weft is more diversified, and the woven fabric is more rich.

In this study, using ADAMS parametric modeling and ADAMS-ANSYS combined rigid flexible coupling analysis is to optimize the design of the spatial four bar weft insertion mechanism from two aspects of kinematic parameters and structural stiffness improvement, which provided theoretical basis for further analysis and optimization of the mechanism.

2. Kinematic analysis and simulation verification of weft insertion mechanism

The spatial four-bar weft insertion mechanism [2] is shown in Fig. 1.

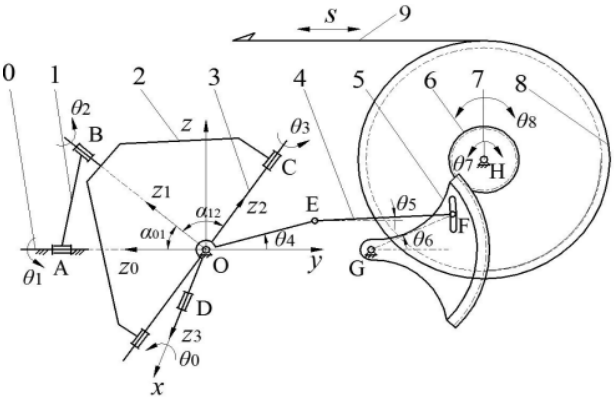

Fig. 1 Spatial four-bar weft insertion mechanism

From Fig. 1, *0* is a box; *1* is crank; *2* is a fork connecting rod; *3* is the cross cycloidal axis; *4* is the connecting rod; *5* is a sector gear; *6* is a transmission gear; *7* is rapier wheel; *8* is a rapier band.

In Fig. 1, the output motion of the motor is input to the weft insertion mechanism system at place A, which drives the crank *1* to perform integral turnover, thus driving the fork connecting rod *2* to perform complex spatial motion. The cross pendulum shaft *3* reciprocates under the constraint of box *0* and driven by the fork connecting rod *2*, namely, the output motion of the space 4R mechanism. Though the planar four - bar mechanism OEFG, drive the sector gear *5* to do reciprocating swing; Fan gear *5* is provided with a chute, the *F* end of connecting rod *4* can move in the chute, thereby indirectly changing the distance between the hinge point *F*, *G* to adjust the rapier drive; After the motion amplification of transmission gear *6* and rapier

wheel *7*, the motion is transferred to rapier belt *8*. rapier belt *8* makes reciprocating linear motion to realize weft insertion.

2.1. Kinematic modeling

Firstly, the space 4R mechanism was analyzed to establish the relationship between output angle θ_0 and input angle θ_0. Bar *2* is hypothetically disassembled, combined with the knowledge of space mechanism, and the direction cosine matrix method [3] is adopted to obtain the following relation:

$$(0,0,1)[C_{23}][C_{30}][C_{01}](0,0,1)^T = cos\alpha_{12}. \quad (1)$$

Substitute it into the coordinate system transformation matrix, and after simplification, it can be obtained:

$$\theta_0 = 2arctan\frac{A_1 + \sqrt{A_1^2 + B_1^2 - C_1^2}}{B_1 - C_1}, \quad (2)$$

where: $A_1 = -cos\theta_1$; $B_1 = \frac{cos\alpha_{01}}{sin\alpha_{01}}$; $C_1 = \frac{cos\alpha_{12}}{sin\alpha_{01}}$; α_{01} is the angle between Z_0 and Z_1.

By analyzing the geometric relationship in Fig. 1, we can obtain:

$$\theta_4 = \theta_0 - \alpha_{COE}, \quad (3)$$

where: α_{COE} is the angle between CO and OE in the cycloidal axis of the cross; θ_4 is the angle between OE and the positive direction of the *Y* axis of the fixed coordinate system.

In the fixed coordinate system OXYZ shown in Fig. 1, according to the geometric relationship, we can obtain:

$$\begin{cases} L_{OE}cos\theta_4 + L_{EF}cos\theta_5 = L_{OG} + L_{FG}cos\theta_6 \\ L_{OE}sin\theta_4 + L_{EF}sin\theta_5 = L_{FG}sin\theta_6 \end{cases}, \quad (4)$$

where: L_{OE}, L_{EF}, L_{FG}, L_{OG} is the distance between hinged points *O* and *E*, *E* and *F*, *F* and *G*, *O* and *G*, mm; θ_5 is the angle between *EF* and the positive direction of *Y* axis of the fixed coordinate system; θ_6 is the angle of fan gear. By simplifying Eq. (4), the relation between θ_6 and θ_4 can be written as:

$$\theta_6 = 2arctan\frac{-A_2 \pm \sqrt{A_2^2 + B_2^2 - C_2^2}}{C_2 - B_2}, \quad (5)$$

$$A_2 = -2L_{FG}L_{OE}sin\theta_4, \quad (6)$$

$$B_2 = 2L_{FG}\left(L_{OG} - L_{OE}cos\theta_4\right), \quad (7)$$

$$C_2 = L_{OE}^2 + L_{FG}^2 + L_{OG}^2 - L_{EF}^2 - 2L_{OE}L_{OG}cos\theta_4. \quad (8)$$

Output motion function, plus and minus sign according to the actual mechanism diagram and continuity of motion. Judgment takes a positive sign. Analyze the assembly relationship of sector gear *5*, transmission gear *6*, rapier wheel *8* and rapier belt *9* in Fig.1. According to the actual assembly scheme and movement continuity, the minus sign is taken in Eq. (5). According to the assembly relationship of sector gear, transmission gear, rapier wheel and rapier belt, the displacement equation of rapier belt can be obtained as follows:

$$s = \frac{d_5 d_7 \theta_6}{2d_6}, \quad (9)$$

where: d_5 is the sector gear indexing circle diameter, mm; d_6 is the dividing circle diameter of transmission gear, mm; d_7 is the rapier wheel indexing circle diameter, mm. The derivative of the belt displacement with respect to time gives the velocity and the acceleration of the belt.

2.2. Kinematics simulation verification analysis

By modeling each member of the weft insertion mechanism in 3D, and according to the position relationship of each member in Fig. 1, the model of the built part is virtually assembled, and the parameter measurement of the assembly is carried out using the measurement function.

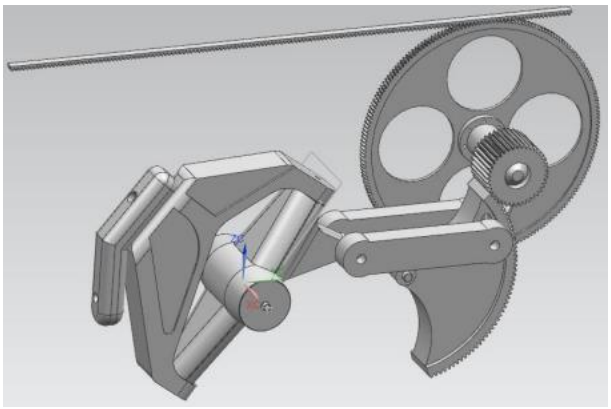

Fig. 2 Three dimensional model of the spatial four-bar weft insertion mechanism

The motion geometric parameters for each component are shown in Table 1.

Table 1

Kinematic geometric parameters of each component

Parameter name	Parameter value
Angle α_{01}, ° between Z_0 and Z_1	40
Angle α_{12}, ° between Z_1 and Z_2	85
Angle α_{COE}, ° between *CO* and *OE*	39
Distance L_{OE}, mm between hinge points *E* and *F*	228.34
Distance L_{OE}, mm between hinge points *F* and *G*	146.04
Distance L_{OE}, mm between hinge points *O* and *E*	181.5
Distance L_{OG}, mm between hinge points *O* and *G*	265.53
Diameter of indexing circle of sector gear d_5, mm	356.1
Diameter of indexing circle of sector gear d_6, mm	59.35
Diameter of indexing circle of sector gear d_7, mm	386

The author applies MATLAB software and combines theoretical analysis to obtain the relation of rapier belt motion function [4]. It is assumed that the rotation speed of the crank is 400 r/min. One week of crank rotation is defined as a cycle. According to the measured motion geometric parameters in Table 1, the motion regularity curve of the rapier belt within a motion cycle is obtained, and the results are compared with the ADAMS simulation results.

When the spindle rotation angle is 0°~50°, the rapier belt movement is relatively gentle. At this time, the rapier head picks up yarn to prepare for yarn feeding movement. The gentle movement is conducive to stable and accurate yarn picking. When the spindle rotation angle is 50°~115°, the loom executes yarn feeding. In order to ensure the work efficiency, the speed of rapier belt reaches the peak at this stage, and the acceleration fluctuates greatly, which meets the requirements of fast yarn feeding. When the rotation angle of the main shaft is 115°~245°, the acceleration of the rapier belt is relatively gentle at this stage, without violent fluctuation. At this time, the loom is in the process of filling handover, which requires small acceleration fluctuation to ensure smooth filling joint. When the spindle rotation angle is 245°~310°, the weft handover work is finished and the loom is in the stage of the blade he-ad return. In this case, it is necessary to quickly rewind the blade to improve work efficiency.

When the spindle rotation angle is 310°~360°, the loom will pick up the yarn again to prepare for the next weft insertion. In this stage, the speed fluctuation should not be too large. The comparison curve of rapier belt motion law is basically in line with the requirement of weft insertion process, which proves the correctness of 3D modeling and simulation analysis. In addition, it can be seen from Fig. 3 that the results of theoretical calculation and software simulation are highly consistent, and the errors are within a reasonable range.

Therefore, the correctness of the kinematic modeling is proved, which provides a correct theoretical basis for the discussion of the influence of geometric parameter changes on the kinematic performance of the rapier belt and the optimization analysis of the weft insertion mechanism.

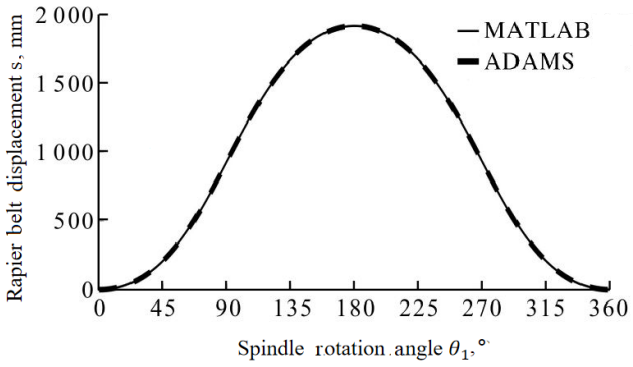

a

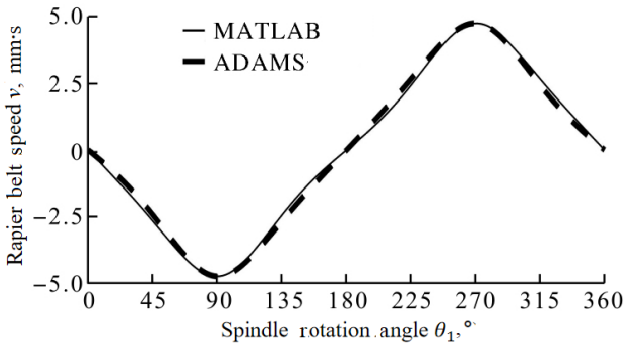

b

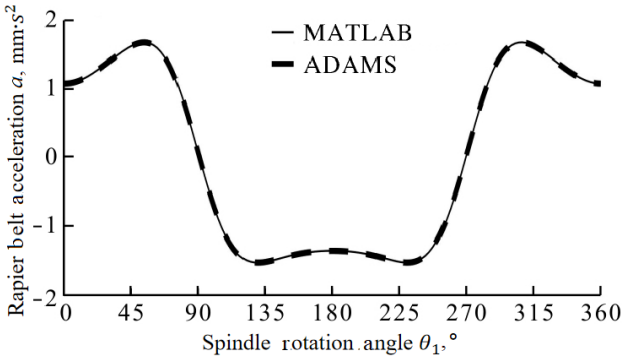

c

Fig. 3 a) Comparison of theoretical and simulation curves of rapier belt displacement; b) comparison of theoretical and simulation curves of rapier belt speed; c) comparison of theoretical and simulation curves of rapier belt acceleration

3. Dynamic optimization of rigid body based on stationary motion

3.1. Establishment of optimization model

According to the kinematics analysis of the weft insertion mechanism and the actual situation, the design variables were selected as follows:

$$X = \{x_1, x_2, x_3\} = \{\alpha_{01}, \alpha_{12}, L_{FG}\}. \tag{10}$$

The minimization of the maximum acceleration of the rapier belt is set as the optimization objective, which can be expressed as:

$$F(x) = |a_{max}| \rightarrow min. \tag{11}$$

At the same time, the unilateral performance should not be pursued too much, while the influence on other conditions should be ignored. Some other kinematic performance and size requirements of the weft insertion mechanism should also be met, so the constraint conditions are set as follows:

1. Maximum motion requirements of rapier belt:

$$s_{max} \geq 1500 \text{ mm}, \tag{12}$$

2. Existence condition of space 4R mechanism crank:

$$\alpha_{01} \leq \alpha_{12}. \tag{13}$$

3. Double rocker mechanism rod length condition:

$$L_{FG} + L_{OG} \geq L_{OE} + L_{EF}. \tag{14}$$

3.2. ADAMS optimization experiment and result analysis

In ADAMS, the author ignores the geometric shape of each component, and establishes a parameterized model of weft insertion mechanism by establishing parameterized points and replacing each component with simple connecting rods.

In ADAMS, the geometric shape of each component is ignored, and the parametric model of the weft insertion mechanism is established by establishing parameterizable points and replacing each component with a simple connecting rod. Before you start optimizing your design, first set the design variables. The length of LFG is determined by the position of the hinge point F, and the corresponding design variable is changed to the Angle between the connecting rod EF and the positive direction of the Y axis for the convenience of analysis. The length of LOE and LEF can be changed by changing the y coordinate of the hinged point E.

Before you start optimizing your design, set your design variables. Wherein, the length of LFG is determined by the position of hinge point F. For convenience of analysis, its corresponding design variable is changed to the angle between connecting rod EF and the positive direction of Y-axis. Design variables and their value ranges are shown in Table 2.

Table 2

Design variables and value ranges

Design variable	Value range
$DV\_\ \alpha_{01}$, °	30~45
$DV\_\ \alpha_{12}$, °	70~90
$DV\_\ \alpha_{EFY}$, °	-5~5
DV_E_y, mm	-30~20

The coordinate values of key design points point_B, point_C and point_F are parameterized and expressed by design variables. Then, the acceleration of the rapier belt is measured, and the maximum value in the simulation process is set as the objective function OBJECTIVE_1 of optimization analysis. According to the constraints analyzed above, corresponding constraint equations OPT_CONSTRAINT_1/2/3 are set respectively. Run the Design Evaluation Tools function in ADAMS, set the target to minimize the target function, select design variables and constraints, select OPTDESGRG optimization algorithm, and run the optimization command. Taking the rotary crank as an example, the flexible rigid flexible coupling simulation model is shown in Fig. 4.

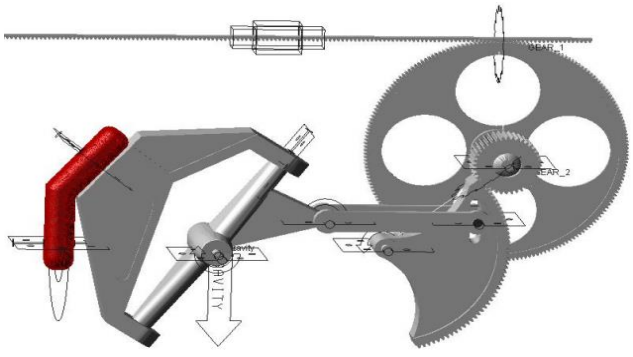

Fig. 4 The rotary crank is a rigid-flexible coupling model of flexible body

By optimizing the three variables at the same time, a set of optimal motion parameters can be obtained through iterative calculation. The optimization results are shown in Table 3.

As can be seen from Table 3, a group of optimal motion parameters can be obtained through iterative calculation when the three variables are optimized at the same time. The maximum acceleration of the target rapier belt is optimized from 1.71e+06 mm/s^2 to 1.0999e+06 mm/s^2. At the same time, the maximum displacement of rapier belt is reduced from 1914 mm to 1500 mm. The comparison curve before and after optimization is shown in Fig. 4.

Table 3

Comparison of optimization results

Design variable	Before optimization	After optimization
$DV\_\ \alpha_{01}$, °	40	30.9207
$DV\_\ \alpha_{12}$, °	80	90
$DV\_\ \alpha_{FEY}$, °	0	-2.17681

According to the analysis of Fig.5, under the condition that the driving distance of the rapier is greater than or equal to 1500 mm, the maximum acceleration of the rapier belt decreases by about 35.7%, and the motion stability of the rapier belt is significantly improved. The acceleration motion curve tends to be more isosceles trapezoid, and the acceleration changes more gently at the junction of yarn and weft, thus achieving smooth weft joint [5].

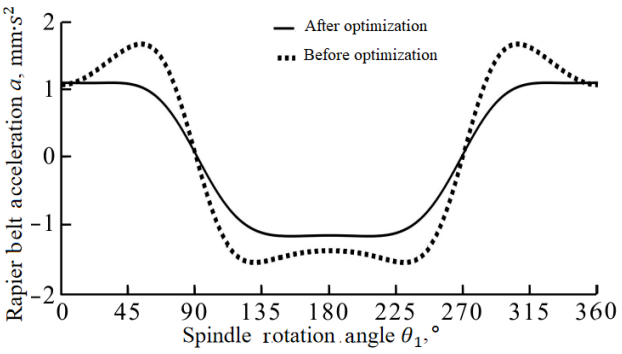

a

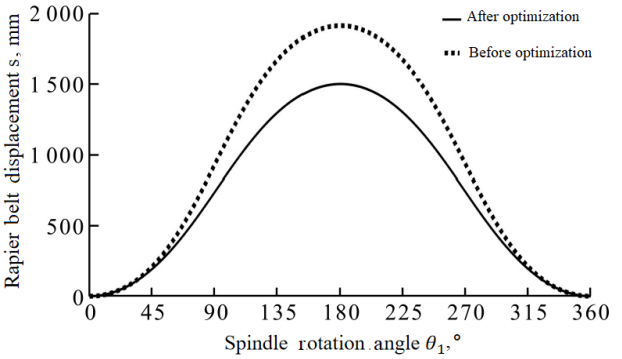

b

Fig. 5 a) Comparison of rapier belt acceleration curves before and after optimization; b) comparison of rapier displacement curves before and after optimization

4. Structure optimization based on motion accuracy requirements

As rapier loom works at high speed, the flexible deformation of some components is large, which seriously

affects the motion accuracy of the rapier belt. The full rigid body dynamics analysis of the weft insertion mechanism is not enough to reflect the real working condition of the mechanism, so the author puts forward the cosimulation method of ADAMS and ANSYS [6-9]. The rigid-flexible coupling simulation analysis of rapier loom weft insertion mechanism is carried out.

Compared with the displacement and velocity of the rapier belt [10], the flexible deformation of components has the greatest influence on the acceleration of the rapier belt. At present, the author makes each component flexible and establishes the rigid-flexible coupling model respectively. Through simulation, the error curve of the rapier belt acceleration when each component is flexible is obtained, and structural optimization design is carried out for the corresponding component with the largest error.

4.1. Establishment of rigid-flexible coupling model

The author will export the flexible component from UG (UG is a mold design software) to x_t format file, and import the generated file into ANSYS. The density is set to 7801 kg/m^3, elastic modulus is set to 207 GPa, Poisson's ratio is set to 0.29, and grid division is carried out by SOLID185 and MASS21. A rigid area is established at the connection with other members for the addition of motion pairs in ADAMS; The first 6 modes of the rigid region are extracted, and finally the MNF neutral file is derived. In ADAMS, the flexible body is used to replace the corresponding rigid parts, redefine the motion pair, and finally get the rigid-flexible coupling simulation model.

4.2. Rigid-flexible coupling dynamics simulation analysis

In ADAMS, the rigid-flexible coupling model was driven, the motor speed was also set at 400 r/min, and the simulation time was 0.15 s. According to the actual working condition of the weft insertion mechanism, the rapier belt drives the rapier head to reciprocate motion, so a vertical downward concentrated load is applied at the end of the rapier belt. The load size is determined by the mass of the rapier head, which is set as 4 N here.

The rigid-flexible coupling model of each component is simulated in turn. Among them, the acceleration error of rapier belt caused by the flexibility of sector gear, transmission gear, rapier wheel and rapier belt is relatively small, which will not be discussed here.

The large fluctuation of the rapier belt acceleration will have a large impact force on the yarn, which is easy to break the yarn and affect the stability of the weft insertion. When the spindle angle is between 115°and 245°, the acceleration of the sword belt fluctuates sharply. When the spindle angle is within this range, the weft handover is being carried out between the weft feeding head and the weft picking head. If the acceleration fluctuates violently, the weft handover will fail, and the increase of inertia force will lead to the increase of impact force, thus damaging the weft head and the weft line. In order to analyze the rapier belt acceleration error caused by the flexibility of the member more deeply, the two curves are subtracted to get the rapier belt acceleration error curves when the rotary crank is flexible. Similarly, we no longer analyze the displacement and velocity of the belt when the fork connecting rod, the cross pendulum shaft and the connecting rod are flexible, but only analyze the acceleration error of the belt when they are flexible. The acceleration error curves of rapier belt are obtained when each member is flexible.

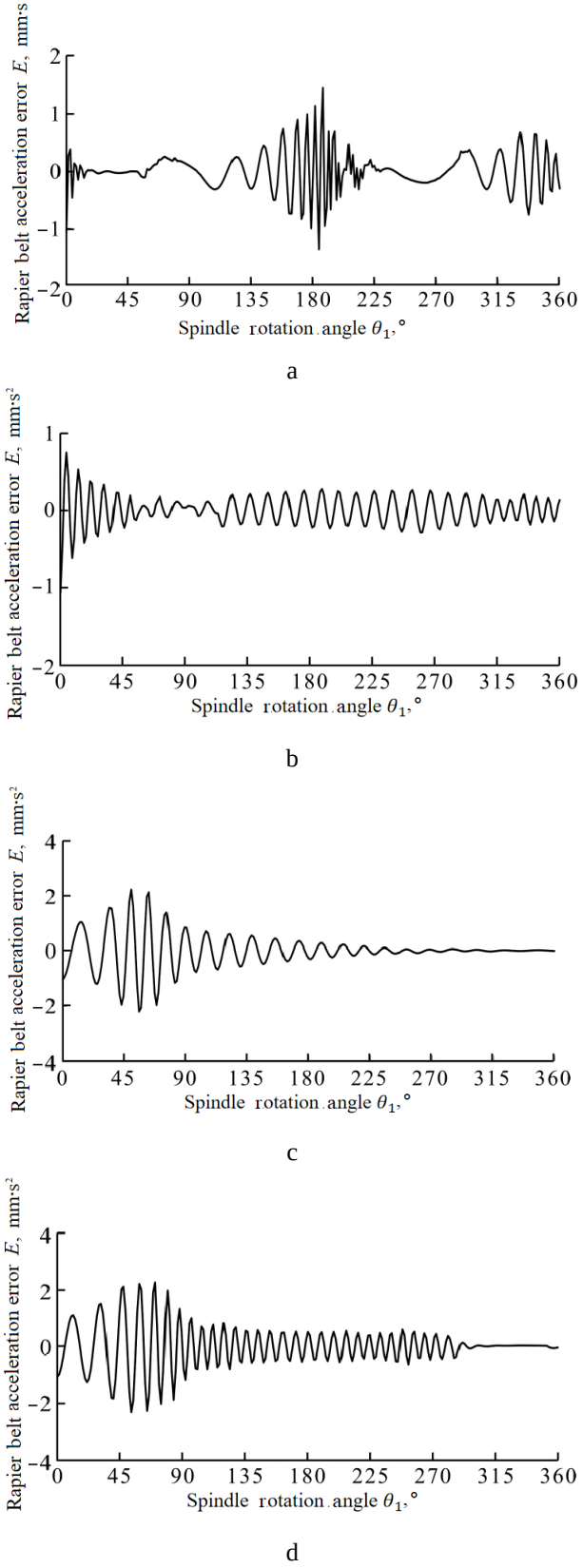

Fig. 6 a) Rapier belt acceleration error curve when the crank is flexible; b) rapier belt acceleration error curve when the fork connecting rod is flexible; c) rapier belt acceleration error curve when the cross pendulum shaft is flexible; d) rapier belt acceleration error curve when the linkage is flexible

The acceleration error curves of rapier belt obtained by simulation when each component is flexible is shown in Fig. 6.

It can be seen from the analysis of Fig. 5 that the flexibility of each component will affect the motion accuracy of the rapier belt, thus affecting the stability and accuracy of yarn and weft handover. Among them, the flexibility of the connecting rod has the most significant influence on the acceleration of the rapier belt, so it is necessary to take the connecting rod as an example to optimize its structure.

4.3. Structure optimization experiment and result analysis

In view of the influence of flexible connecting rod on the accuracy of rapier belt motion, the author proposes to increase the section size of connecting rod to improve its structural stiffness and reduce the influence of flexible deformation on the acceleration of rapier belt. The width and thickness of the connecting rod were increased by 10 mm each time, and the structure of the connecting rod was optimized twice [11-13]. The parameter pairs before and after connecting rod optimization are shown in Table 4.

Table 4

Comparison of parameters before and after connecting rod optimization

Optimization object	Before optimization	After first optimization	After secondary optimization
Connecting rod width, mm	36	46	56
Connecting rod thickness, mm	16	26	36

The author imported the optimized connecting rod into ANSYS for flexibility processing, and then carried out rigid-flexible coupling simulation analysis in ADAMS. According to the analysis of Fig. 5, d, when the spindle angle is between 0°and 90°, the error is relatively large. In order to clearly compare the errors before and after optimization, only the comparative analysis of rapier belt acceleration errors before and after optimization when the spindle angle is within the interval 0°~90°is shown here.

The comparison curve of rapier belt acceleration errors before and after connecting rod optimization is shown in Fig. 7.

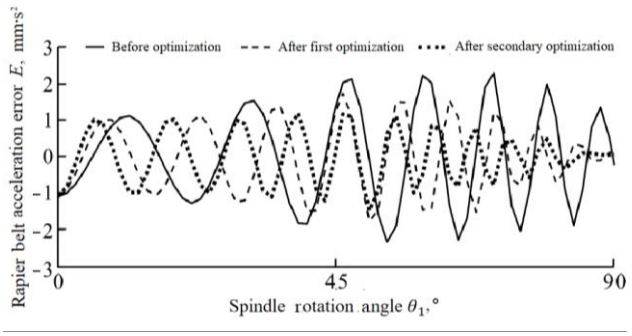

Fig. 7 Comparison curve of belt acceleration error before and after rod optimization

As can be seen from Fig. 7, when the section size of connecting rod is increased, the motion error of rapier belt decreases accordingly. The larger the section size is, the smaller the acceleration error of rapier belt is. This proves the effectiveness and feasibility of the optimization method.

5. Conclusion

The dynamic performance of the weft insertion mechanism of the rapier loom is the key to ensuring the reliability of the overall performance of the loom and the quality of the fabric. Given the motion stability and motion accuracy of the spatial four-bar weft insertion mechanism, the author carried out the optimization design from two aspects:

To minimize the maximum acceleration of the rapier belt, using ADAMS parametric modeling was adopted for optimization analysis, a group of optimal motion parameters was finally obtained, and the maximum acceleration of the optimized rapier belt was reduced by 35.7 %. The acceleration curve shape was more inclined to an isosceles trapezoid, and the stability of the rapier belt motion was improved.

2. Considering the flexible deformation of the weft insertion mechanism of the rapier loom, the rigid-flexible coupling simulation analysis of the weft insertion mechanism was carried out. Through structural optimization of the connecting rod, the structural stiffness of the competent was increased to reduce the impact of its flexible deformation on the motion accuracy of the rapier belt, and the acceleration error of the optimized rapier belt was significantly reduced.

The optimization results revealed that the motion stability of the rapier belt was improved. The movement error caused by the flexible deformation of the component was significantly reduced. The motion accuracy of the rapier belt was improved, and the dynamic performance of the weft insertion mechanism was significantly enhanced. The results provide a theoretical basis for further analysis and optimization of the mechanism.

However, the optimization effect between this method and the introduced optimization algorithm needs to be further compared in the future.

Acknowledgments

This work is supported by the General Project of National Natural Science Foundation of China (nos. 52075 110) and by the Key Project of Natural Science Foundation of Guangxi, China (Num.2023GXNSFDA026045).

References

1. **Mutschler, T.; Weber, M. O.; Bueno, M. A.** 2022. Process analysis and outlook for the development of a new weft yarn inlay system for warp knitting, Journal of Engineered Fibers and Fabrics p. 17. http://dx.doi.orgdoi:10.1177/15589250221101388.
2. **Eren, R.; Erturk, M.; Hascelik, B.** 2014. Kinematic design and motion analysis of spatial rapier drive mechanisms used in weaving machines, Textile Research Journal 84(19): 2065-2073. https://doi.org/10.1177/0040517514534754.
3. **Genel, Ö. E.; Tüfekci, M.; Tüfekci, E.** 2022. Free vibrations of spatial frame structures: analytical modelling and solution, Journal of Vibration and Control. https://doi.org/10.1177/10775463221122086.
4. **Gauhar, A.; Rashid, A.; Hasan, O.; Bispo, J.; Cardoso, J. M.** 2021. Formal verification of Matrix based

MATLAB models using interactive theorem proving, Peer J. Computer Science 7: e440. https://doi.org/10.7717/peerj-cs.440.
5. **Liu, Y.; Fu, L.; Zhao, Z.; Ma, Q.; Rui, Y.; Zhang, Z.** 2022. Analysis of the coaxiality-geometric hysteresis model of a rotate vector reducer based on Ansys Adams, Mechanical. Sciences 13: 855–866. https://doi.org/10.5194/ms-13-855-2022, 2022.
6. **Dukalski, P.; Będkowski, B.; Parczewski, K.; Wnęk, H.; Urbaś, A.; Augustynek, K.** 2022. Analysis of the influence of motors installed in passenger car wheels on the torsion beam of the rear axle suspension, Energies 15: 222. https://doi.org/10.3390/en15010222.
7. **Qiao, X.; Shunqi, M.; Xiaoyu, Y.** 2019. Analysis of the magnetic field and electromagnetic force of a non-striking weft insertion system for super broad-width looms, based on an electromagnetic launcher, Textile Research Journal 89(21-22): 4620-4631. https://doi.org/10.1177/0040517519839371.
8. **Xiao, L.; Zhang. S.** 2017. Analysis and optimization of drum washing machine vibration isolation system based on rigid-flexible virtual prototype model, Journal of Vibroengineering 19(3): 1653-1664. https://doi.org/10.21595/jve.2017.17851.
9. **Wang, Z.; Zhao, J.; Zeng, G.** 2022. Modeling, simulation and implementation of all terrain adaptive five DOF robot, Sensors 22: 6991. https://doi.org/10.3390/s22186991.
10. **Zhang, Z.; Wang, X.; Lu, J.; Qian, K.; Zhang, J.; Zhang, D.** 2022. Interfacial, tensile and bending properties of a novel wide angle woven fabric/EPDM composite, Journal of Industrial Textiles 2022: 52. https://doi.org/10.1177/15280837221121937.
11. **Li, Y.; Zhang, Z.; Xu, L.** 2022. Multi-objective structural optimization of the aluminum alloy subway car body based on an approximate proxy model, Advances in Mechanical Engineering 14(5). https://doi.org/10.1177/16878132221098898.
12. **Besset, S.; Jezequel, L.** 2005. Modal analysis of hollow parts of a structure, IMAC XXIV: A Conference and Exposition on Structural Dynamics. https://doi.org/10.1142/S0218396X08003592.
13. **Zhu, Y.; Ni, L.; Zhang, J.** 2018. Numerical analysis and optimal design of the breechblock mechanism, Advances in Mechanical Engineering 10(2). https://doi.org/10.1177/1687814018762472.

M. Xi, K. Zhou, X. Zhang, X. Lu

OPTIMIZATION OF MOTION PARAMETERS AND STRUCTURAL STIFFNESS OF SPATIAL FOUR-BAR WEFT INSERTION MECHANISM OF PAPIER LOOM

S u m m a r y

Aiming at the problems of the poor motion stability and low motion accuracy of the rapier belt of the spatial four bar weft insertion mechanism, the optimization design of the mechanism was studied from two aspects of motion parameters and structural stiffness. Firstly, the motion law of the rapier belt is analyzed by using the theory of space mechanism, and its correctness is verified by software simulation, which provides a theoretical basis for the optimization design. Then, with the goal of minimizing the maximum acceleration of the rapier belt and the constraint condition of satisfying the weft insertion process and performance requirements, the parametric modeling of ADAMS was used to optimize the mechanism. Considering the flexibility of the weft insertion mechanism at high speed, a rigid-flexible coupling model was established and simulated, and the influence of the flexible deformation of each component on the motion accuracy of the rapier belt was analyzed. Finally, taking the connecting rod as an example, aiming at reducing the acceleration error of the rapier belt, a method was proposed to reduce the influence of flexible deformation by increasing the section size and structural stiffness. The results show that the maximum acceleration of the belt decreases by 35.7% after optimizing the motion parameters, and the motion stability is improved. After optimizing the structure stiffness, the acceleration error of the rapier belt is obviously reduced and the motion accuracy is improved.

Keywords: weft insertion mechanism, parametric modeling, rigid and flexible coupling, optimization design, ADAMS.

Received March 16, 2023
Accepted December 3, 2023

This article is an Open Access article distributed under the terms and conditions of the Creative Commons Attribution 4.0 (CC BY 4.0) License (http://creativecommons.org/licenses/by/4.0/).